AGU PUBLICATIONS

JGR

Journal of Geophysical Research: Solid Earth

RESEARCH ARTICLE
10.1002/2016JB013243

Key Points:
- Interseismic geodetic data are used to characterize fault zone elastic properties on the San Francisco Peninsula
- Presence of a compliant fault zone is inferred at Lake San Andreas but not at Black Mountain
- Fault zone lithology plays an important role in compliant fault zone formation

Supporting Information:
- Supporting Information S1

Correspondence to:
K. Materna,
kmaterna@berkeley.edu

Citation:
Materna, K. and R. Bürgmann (2016), Contrasts in compliant fault zone properties inferred from geodetic measurements in the San Francisco Bay area, *J. Geophys. Res. Solid Earth*, *121*, doi:10.1002/2016JB013243.

Received 4 JUN 2016
Accepted 3 SEP 2016
Accepted article online 14 SEP 2016

Contrasts in compliant fault zone properties inferred from geodetic measurements in the San Francisco Bay area

Kathryn Materna[1] and Roland Bürgmann[1]

[1]Department of Earth and Planetary Science, University of California, Berkeley, California, USA

Abstract In crustal fault zones, regions of damaged rock characterized by reduced elastic shear modulus can influence patterns of near-field interseismic deformation. In order to study these compliant fault zones (CFZs) and how they might develop over the lifetimes of faults, we compare two fault segments with contrasting fault age and lithology along the San Andreas Fault in the San Francisco Bay Area. New geodetic measurements of the interseismic velocity fields at each location are used to constrain fault zone parameters through a Markov chain Monte Carlo method. At Black Mountain, in the Santa Cruz Mountains of the San Francisco Peninsula, we do not find evidence for a compliant fault zone; instead, we find that the geodetic data are more consistent with a model of a single fault in a homogeneous elastic half-space. At Lake San Andreas, a younger fault segment 35 km farther north, we find evidence for a compliant fault zone about 3.4 +1.1/−1.4 km wide, containing a shear modulus of about 40% of the shear modulus of the surrounding rock. We also find that the best fitting CFZ model at this location, unlike the best fitting homogeneous half-space model, has a locking depth that agrees well with the observed depth of microseismicity. Based on differences in fault age, cumulative displacement, and lithology between Black Mountain and Lake San Andreas, we infer that lithology plays an important and, in this case, perhaps a dominant role in the accumulation of fault zone damage structures and the development of CFZs over the lifetime of a fault.

1. Introduction

In studies of interseismic crustal deformation, faults are often modeled as dislocations embedded in homogeneous elastic half-spaces [*Savage and Burford*, 1973]. However, increasingly sensitive geodetic measurements of active faults in nature can show deviations from this first-order model. Variations in elastic properties, for example through brittle damage or changes in rock composition, can change a fault's geodetic signature. One important example of a structure that differs from the first-order model of faults is a compliant fault zone (CFZ), or near-fault region of damaged rock characterized by a reduced shear modulus. CFZs have been shown to affect the interpretation of geodetic data for coseismic slip distributions [*Barbot et al.*, 2008] and can affect the type of strong ground motion that structures near the fault zone experience during large earthquakes [*Ben-Zion et al.*, 2015]. Recent studies have also shown a connection between faults with CFZs and faults that can sustain supershear ruptures [e.g., *Huang et al.*, 2016]. In order to fully understand these features, it is important to characterize the CFZ structures around major faults.

Recent studies have investigated CFZs around the world through a variety of geophysical observations. Discontinuous deformation observed after the Izmit and Landers earthquakes on faults away from the main rupture are consistent with the coseismic elastic deformation of CFZs [*Fialko*, 2004; *Hamiel and Fialko*, 2007]. Studies of deformation have also investigated the role of CFZs in producing enhanced strain interseismically near the traces of faults in California [*Chen and Freymueller*, 2002; *Jolivet et al.*, 2009; *Lindsey et al.*, 2013] and in Venezuela [*Reinoza et al.*, 2015]. Furthermore, seismic studies have pointed to the existence of material with low seismic velocity and shear modulus around faults such as the Calico Fault in the Mojave Desert and the central San Andreas Fault (SAF) [*Li et al.*, 2004; *Cochran et al.*, 2009]. *Xue et al.* [2016] also documented the presence of highly permeable, low-rigidity material using data from monitoring wells in a 500 m zone around the SAF. The CFZs that have so far been studied are typically on the order of hundreds of meters to several kilometers wide and display rigidities up to several times lower than the surrounding rocks.

On the northern SAF in particular, previous geodetic studies have found conflicting evidence for low-rigidity fault zones. *Lisowski et al.* [1991] suspected the presence of low-rigidity materials in the fault core at a trilateration profile in Point Reyes, north of San Francisco, California. The electronic distance measurement (EDM) data in their study showed high strain rates that were not easily explained by shallow locking depths or shallow fault creep. *Chen and Freymueller* [2002] analyzed a denser set of EDM and Global Positioning System (GPS) measurements along the northern SAF, finding high strain rates that suggested the presence of a CFZ on the San Francisco Peninsula, but not at Point Reyes where *Lisowski et al.* [1991] had suggested low-rigidity materials. *Jolivet et al.* [2009] used a combination of trilateration, GPS, and Interferometric Synthetic Aperture Radar (InSAR) data to revisit the region north of San Francisco Bay. The results of their work suggest strong variability in the CFZ structures along the SAF, even at small spatial scales. In agreement with earlier results by *Chen and Freymueller* [2002], *Jolivet et al.* [2009] find no evidence for a CFZ for a GPS profile at Point Reyes, but a separate geodetic profile only 30 km north of Point Reyes provides strong support for a CFZ.

In this study, we use new GPS measurements of two geodetic networks previously considered by *Chen and Freymueller* [2002] along the San Francisco Peninsula segment of the SAF. We examine two decades of geodetic measurements to more completely characterize the variations in the CFZ's structure along the SAF. Our study regions are Lake San Andreas (Figure 1a) and Black Mountain (Figure 1b), both located just south of San Francisco. These two areas provide a contrasting case study for CFZ formation through their differences in fault age, lithology, and tectonic setting.

The SAF in northern California in general forms the boundary between the Salinian Block to the west and the San Francisco Bay Block to the east (Figure 1c). The Salinian Block is made up of mostly Cretaceous granites and metamorphic rocks overlain by Tertiary sediments [*Mattinson*, 1978; *James*, 1992]. To the east, the San Francisco Bay Block is a mixture of rocks of the Franciscan complex: mostly sandstone, shale, basalt, chert, and schist derived from the subduction of the former Farallon plate [*Blake and Jones*, 1974]. Plate reconstructions show that the SAF at this latitude, as the primary fault of the plate boundary system, has accommodated about 162 km of right-lateral strike-slip motion over its 12–13 million year lifetime [*Powell*, 1993].

On the San Francisco Peninsula, however, most of the 162 km of right-lateral motion appears to have been accommodated not on the current SAF but on a presently inactive structure called the Pilarcitos Fault, which is west of the SAF and forms the boundary between Salinian and Franciscan rocks [*Parsons and Zoback*, 1997]. Geologic and magnetic studies suggest that slip shifted eastward from the Pilarcitos Fault to the present-day SAF approximately 1.5 million years ago [*Hengesh and Wakabayashi*, 1995; *Jachens and Zoback*, 1999], resulting in a long triangular region of the initial San Francisco Bay Block (hatched region in Figure 1c) currently moving northwest with the Salinian Block and the Pacific Plate. Since the shift of the active fault trace, this region has been displaced about 23 km to the northwest from its original position [*Jachens and Zoback*, 1999].

The SAF segments at both the Black Mountain and Lake San Andreas study areas were affected by the Quaternary shift of the Peninsula SAF to its present position. Lake San Andreas is on a young stretch of the Peninsula SAF, with the blocks to the east and west of the fault both having only 23 km of cumulative displacement over active lifetimes of 1.5 million years. Both sides of the fault zone are lithologically part of the Franciscan complex. At Black Mountain, the western side is a relatively mature fault zone, consisting of Salinian rocks that have seen more than 100 km of cumulative displacement. The eastern side is similar to the young fault zone at Lake San Andreas (most easily seen if one imagines the triangular block in Figure 1c backtracked to the southeast by 23 km, to its position before the active fault shifted) [see *Parsons and Zoback*, 1997, Figure 10]. The two fault zone sections considered in this study therefore have eastern sides that are similar but western sides that differ in both fault age and lithology.

A further difference between the two fault zones is the present-day tectonic environment. The SAF at Black Mountain goes through a restraining bend of approximately 9° just south of the mapped region in Figure 1c, which produces a transpressional environment and uplift of the Santa Cruz Mountains [*Scholz*, 1985; *Anderson*, 1990; *Bürgmann et al.*, 1994]. The focal mechanisms of small earthquakes in this area, which are mainly strike slip and reverse, support the idea that the region is currently in transpression [*Zoback et al.*, 1999]. In contrast, the SAF at Lake San Andreas is thought to be in transtension associated with a slight releasing bend in the fault trace of approximately 5° and with the nearby junction of the San Gregorio fault. The earthquakes along this stretch of the fault are a combination of strike-slip and normal faulting events [*Zoback et al.*, 1999].

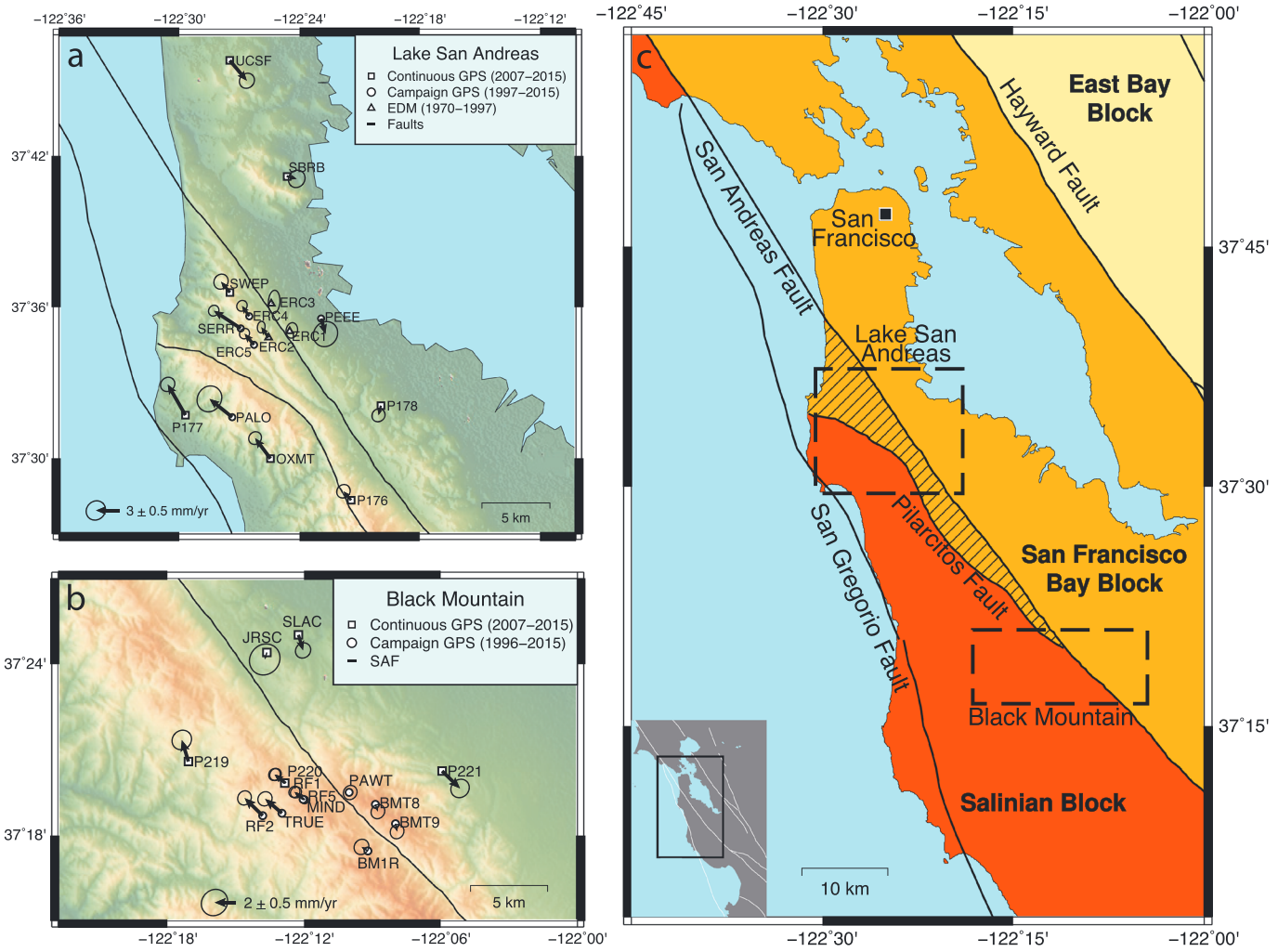

Figure 1. (a) Map of the Lake San Andreas region showing the GPS- and EDM-derived velocities used in this study with 95% confidence ellipses. The velocities are displayed assuming zero velocity at the trace of the SAF. (b) Map of Black Mountain showing the GPS velocities used in this study with 95% confidence ellipses. (c) Simplified geologic map of the San Francisco Bay Area showing the major faults in the region, including the Pilarcitos Fault. The hatched area shows the region of the San Francisco Bay Block that has been offset by the currently active strand of the SAF at Lake San Andreas. The central regions of the Lake San Andreas and Black Mountain geodetic networks are highlighted in the black dashed boxes.

In this study, we use the Black Mountain and Lake San Andreas segments of the SAF to explore the factors that influence the development of CFZs. Because CFZs consist of highly damaged rocks, it is reasonable to expect that mature fault segments accumulate more brittle damage and thus develop broader CFZs over many earthquake cycles. However, it is also possible that rock composition strongly influences the creation of damage structures like CFZs; this factor may be particularly important in the San Francisco Bay Area, where seismic studies have shown differences in seismic wave speed and shear modulus between Salinian and Franciscan rocks [*Parsons and Zoback*, 1997; *Brocher*, 2005; *Thurber et al.*, 2007]. In this study we consider the contrasts between Lake San Andreas and Black Mountain in order to investigate the relationships between fault age, fault lithology, tectonic setting, and the presence of CFZs.

2. Methods

2.1. Data Collection

We collected campaign GPS data at nine geodetic benchmarks at Black Mountain and four benchmarks at Lake San Andreas during the spring and summer of 2015. These benchmarks, all located within 5 km of the surface trace of the SAF, were installed by the U.S. Geological Survey (USGS) in the 1970s for trilateration surveys. Consequently, we have nearly 20 years of EDM measurements from the 1970s to the 1990s, which were analyzed by *Chen and Freymueller* [2002], as well as a time series of campaign GPS measurements at each

benchmark from 1996–1997 to 2015. The campaign GPS time series at Black Mountain typically contain at least four measurements spaced at intervals between 1996 and 2015. At Lake San Andreas, we only have measurements in 1997 and 2015.

During our campaign, we collected data spanning at least two consecutive days at all sites, with data at many sites spanning 5 days or more. Daily position estimates and time series were computed for each site using the GAMIT/GLOBK software package, version 10.6 [*Herring et al.*, 2015]. Nearby continuous sites, mostly from the Plate Boundary Observatory (PBO) and Bay Area Regional Deformation (BARD) networks, were processed jointly with the campaign sites in order to improve network stability. Velocities for all stations (shown in Table S1) were calculated using the ITRF08 reference frame. We produced velocity profiles relative to the SAF by projecting the velocities into the fault-parallel direction and solving for an appropriate offset such that measurements at the fault trace have zero fault-parallel velocity (Figure 1).

At Lake San Andreas, we were unable to locate two benchmarks (ERC1 and ERC3) that we believe have been obscured or destroyed since their last occupation in 1997. At a third site (ERC2), we suspect that the 1997 and 2015 measurements were accidentally made at separate but nearby benchmarks. For these stations, we only have EDM data to constrain their velocities. We converted the EDM line-length data into fault-parallel velocities using the outer coordinate solution [*Prescott*, 1981], which produces a fault-parallel velocity field but is not expressed in an absolute reference frame. We then used the network's stations that have both EDM and GPS measurements to place the EDM data into the reference frame of the GPS data. The velocities calculated by EDM and GPS using this method show good agreement (differences are generally less than 0.5 mm/yr). This agreement implies that there is very little time dependence in the interseismic velocity field between the 1970s and 2015.

2.2. Modeling

We modeled the Black Mountain and Lake San Andreas velocity fields using three possible deformation models. We focused our modeling on measurements within 10 km of the SAF rather than large-scale modeling of the fault system [e.g., *d'Alessio et al.*, 2005], because in the near-field regions of interest, the SAF dominates the deformation signal and contributions from neighboring faults are small. We calculate that the Hayward Fault, located approximately 20 km to the east and slipping at 10 mm/yr, should produce modest deformation gradients of about 0.3 mm/yr across the networks in our study (<0.3 mm/yr if accounting for shallow creep on the Hayward Fault). Similarly, the San Gregorio Fault to the west, which is closer but has a lower slip rate, should produce gradients of about 0.3 mm/yr across each network. The deformation signal from the SAF in this region is an order of magnitude higher. Therefore, we focus only on the deformation related to the SAF and model each velocity field using a single fault for the three candidate crustal models below.

2.2.1. Homogeneous Elastic Half-Space Model

The arctangent model [*Savage and Burford*, 1973] contains a homogeneous elastic half-space with a buried dislocation. The fault-parallel velocity field v, as a function of fault-perpendicular distance from the fault trace x, is modeled by an arctangent function with two parameters: slip rate $\dot{s}$ and locking depth d.

$$v(x) = \frac{\dot{s}}{\pi} \arctan\left(\frac{x}{d}\right)$$

2.2.2. Asymmetric Elastic Half-Space Model

The asymmetric model, detailed in *Le Pichon et al.* [2005] and *Segall* [2010], is an elastic half-space with contrasting shear moduli across the fault (given by μ_1 and μ_2). This model is characterized by three parameters: slip rate $\dot{s}$, locking depth d, and the asymmetry parameter A. The A parameter is defined as $\mu_2/(\mu_1 + \mu_2)$ and is equal to 0.5 when the model has no contrast in rigidity. As defined, this parameter ensures that the portion of the model domain with lower shear modulus experiences higher-amplitude deformation (Figure 2a). This model, like the homogeneous half-space and the CFZ models, has the fault trace located at $x = 0$.

$$x < 0 : v(x) = \frac{2A\dot{s}}{\pi} \arctan\left(\frac{x}{d}\right)$$

$$x \geq 0 : v(x) = \frac{2(1-A)\dot{s}}{\pi} \arctan\left(\frac{x}{d}\right)$$

2.2.3. Compliant Fault Zone Model

The Compliant Fault Zone model is an elastic half-space of shear modulus μ containing a fault zone characterized by a reduced elastic shear modulus μ^* (Figure 2b). This model has four parameters: slip rate $\dot{s}$,

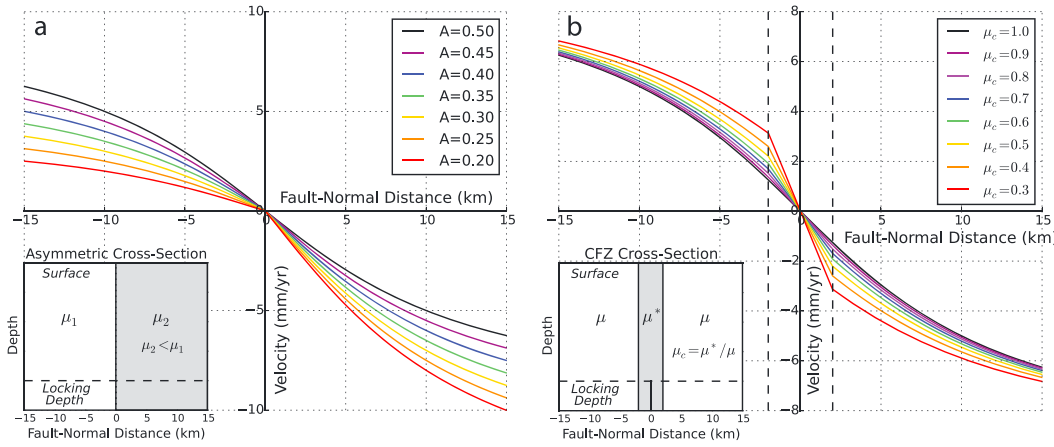

Figure 2. (a) Fault-parallel velocity profiles for an asymmetric elastic half-space model using a range of values for the asymmetry parameter $A = \mu_2/(\mu_1 + \mu_2)$. (b) Fault-parallel velocity profiles for a CFZ model with a 4 km wide fault zone and variable ratio of elastic modulus μ_c.

locking depth d, contrast in shear modulus (expressed as a ratio $\mu_c = \mu^*/\mu$, which ranges from 0 to 1), and half width w of the fault zone. The analytical solutions for the velocity field are from *Rybicki and Kasahara* [1977] and from *Segall* [2010]. A parameter k is defined as $(\mu - \mu^*)/(\mu + \mu^*)$.

$$x \le -w : v(x) = \frac{2(1-k)\dot{s}}{\pi} \sum_{n=0}^{\infty} k^n \arctan\left(\frac{x-2nw}{2d}\right)$$

$$-w < x < w : v(x) = \frac{\dot{s}}{\pi}\left[\arctan\left(\frac{x}{2d}\right) + \sum_{n=1}^{\infty} k^n \left[\arctan\left(\frac{x-2nw}{2d}\right) + \arctan\left(\frac{x+2nw}{2d}\right)\right]\right]$$

$$x \ge w : v(x) = \frac{2(1-k)\dot{s}}{\pi} \sum_{n=0}^{\infty} k^n \arctan\left(\frac{x+2nw}{2d}\right)$$

In each case, the fault was modeled as a vertical, infinitely deep dislocation below the locking depth. CFZs in nature, formed as damage zones in earthquakes, are likely no deeper than the locking depth of the fault.

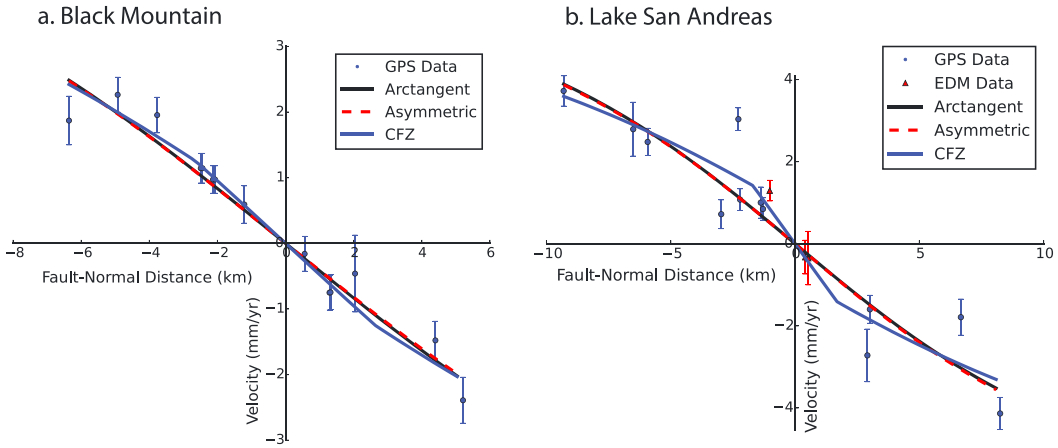

Figure 3. (a) Black Mountain fault-parallel (N39°W) GPS velocities with 1 sigma confidence intervals and best fitting candidate models. The arctangent model is shown in a solid black line; the asymmetric model, which produced very similar results to the arctangent model, is shown in a dashed red line, and the CFZ model is shown in solid blue. (b) Lake San Andreas fault-parallel GPS and EDM (N35°W) velocities with 1 sigma confidence intervals. The solid and dashed curves show the best fitting candidate models for the geodetic data set. Figures 3a and 3b are shown overlaid on the same plot in the supporting information (Figure S1).

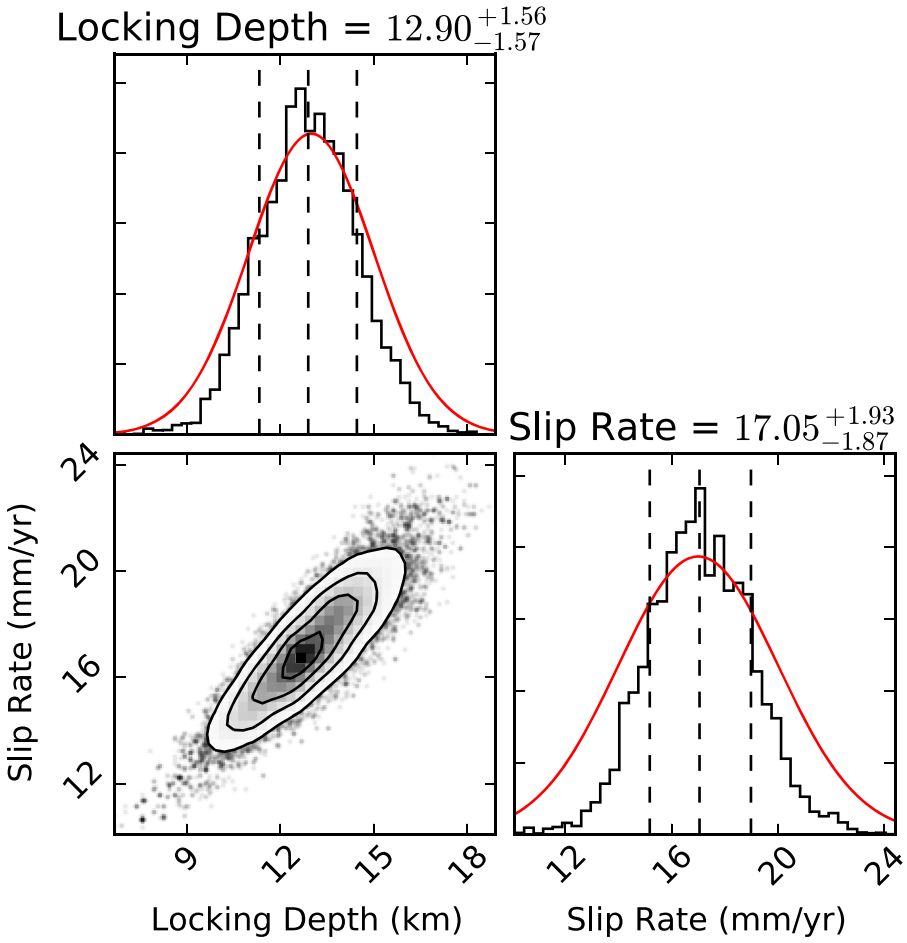

Figure 4. Results of arctangent (homogeneous elastic half-space) modeling at Black Mountain. The black histograms show posterior probability distributions for the slip rate and locking depth, with the dashed lines indicating the 1 sigma (68%) error bounds on each parameter. The red curves show the prior distributions derived from UCERF-3 (13 ± 2 km for locking depth and 17 ± 3 mm/yr for slip rate). The lower left plot shows the trade-off between slip rate and locking depth. The contours on the trade-off diagram show the joint probability distribution, delineating regions with 11%, 39%, 68%, and 86% of the maximum probability value.

Jolivet et al. [2009] found that finite-element modeling of a CFZ with depth equal to the locking depth changed the predictions of surface deformation by less than 5% of the far-field velocity compared to an infinitely deep CFZ. The results the finite-depth CFZ show a narrower and steeper velocity gradient across the fault than the infinitely deep CFZ model, but the differences never exceed 1 mm/yr [*Jolivet et al.*, 2009]. Because the differences are small, we performed model comparisons using the analytical solutions for an infinitely deep CFZ and dislocation for this study.

For each model and study area, we identified best fit parameter values of slip rate, locking depth, etc., using a Markov Chain Monte Carlo (MCMC) method [*Metropolis et al.*, 1953; *Patil et al.*, 2010]. This method was chosen for its ability to identify regions of the parameter space with high probability given the observed data, while also allowing for the use of prior information using Bayes' Rule [*Bayes*, 1763]. In the case of our analysis, the prior information was derived from independent data sources such as geologic slip rate estimates and the depth extent of seismicity. We chose prior distributions for slip rate and locking depth based on the UCERF-3 [*Field et al.*, 2014] fault model (17 ± 3 mm/yr slip rate on the San Andreas Fault and 13 ± 2 km locking depth). These values are in close agreement with block modeling results using GPS velocities [*d'Alessio et al.*, 2005]. Because we had no initial information about the asymmetry or compliant fault zone properties, we chose uniform priors for these parameters. The MCMC algorithm was then used to generate posterior probability distributions for each parameter, including maximum posterior probability values and uncertainty estimates. We also analyzed the trade-offs between parameters in each model.

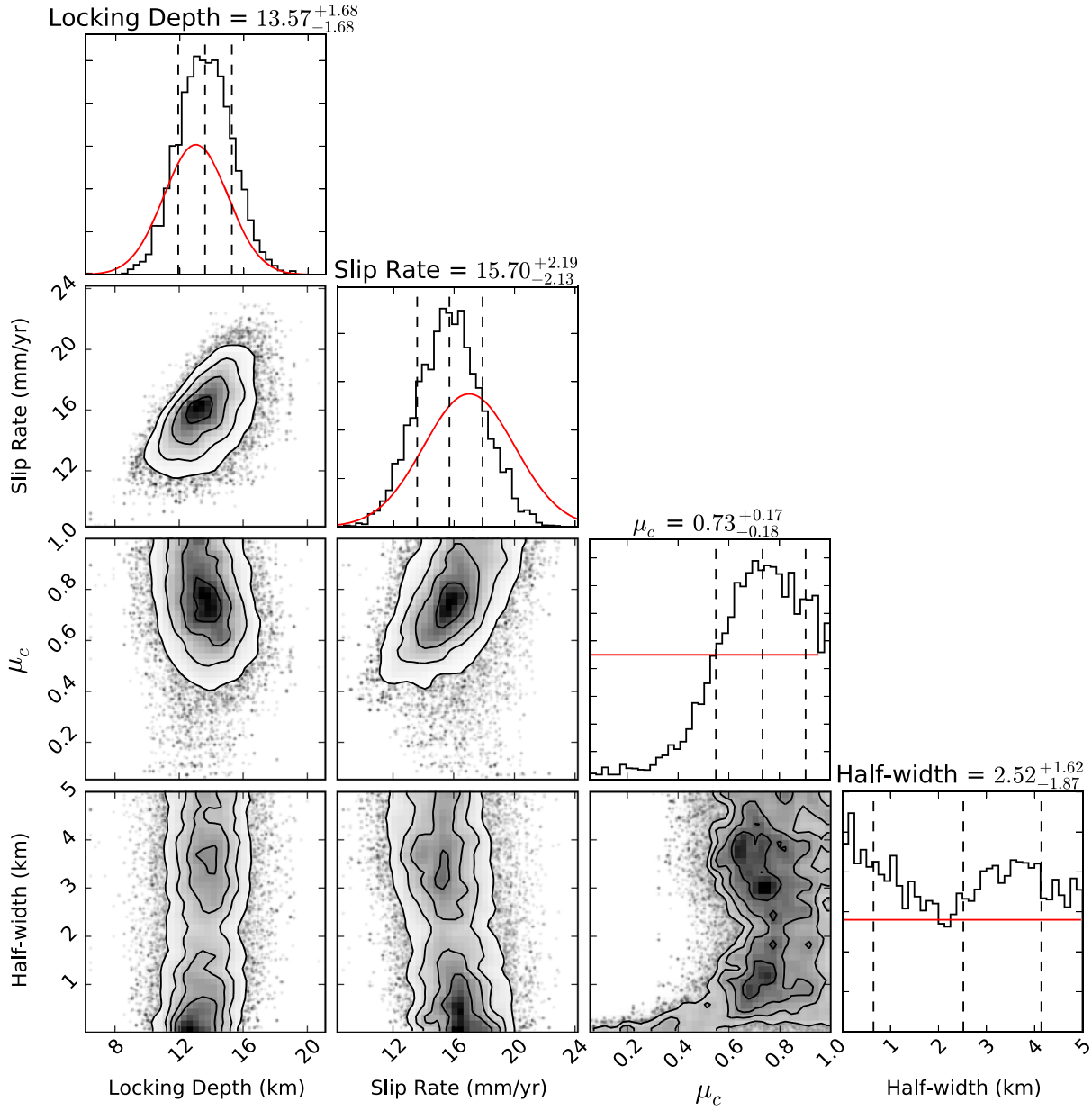

Figure 5. Results of CFZ modeling at Black Mountain. The black histograms show posterior probability distributions for the slip rate, locking depth, contrast in shear modulus, and half width of the CFZ, with the dashed lines indicating the 1 sigma (68%) error bounds on each parameter. The red curves show the prior distributions, derived from UCERF-3 models or otherwise assumed to be uniform. The lower plots show trade-offs between the various parameters.

For each study area, we used the Bayes factor to select the best of the three candidate models in a Bayesian framework [*Kruschke*, 2015]. This technique compares a model $M1$ to a different model $M2$ by calculating the likelihood of producing the observed data set under each model. The Bayes factor, K, is defined as the ratio of the probabilities of observing the data under each model:

$$K = \frac{\int Pr(\theta_1|M1)Pr(D|\theta_1, M1)d\theta_1}{\int Pr(\theta_2|M2)Pr(D|\theta_2, M2)d\theta_2}$$

K is computed as an integral over the entire parameter space, θ, of each model, thus imposing a natural penalty on more complex models with larger parameter spaces. A common interpretation of the Bayes factor is that the data show "substantial" support for Model 1 when the Bayes factor is greater than 3 and "substantial" support for Model 2 when the Bayes factor is less than 1/3 [*Jeffreys*, 1961]. A Bayes factor of 1 shows that the two models are equally probable.

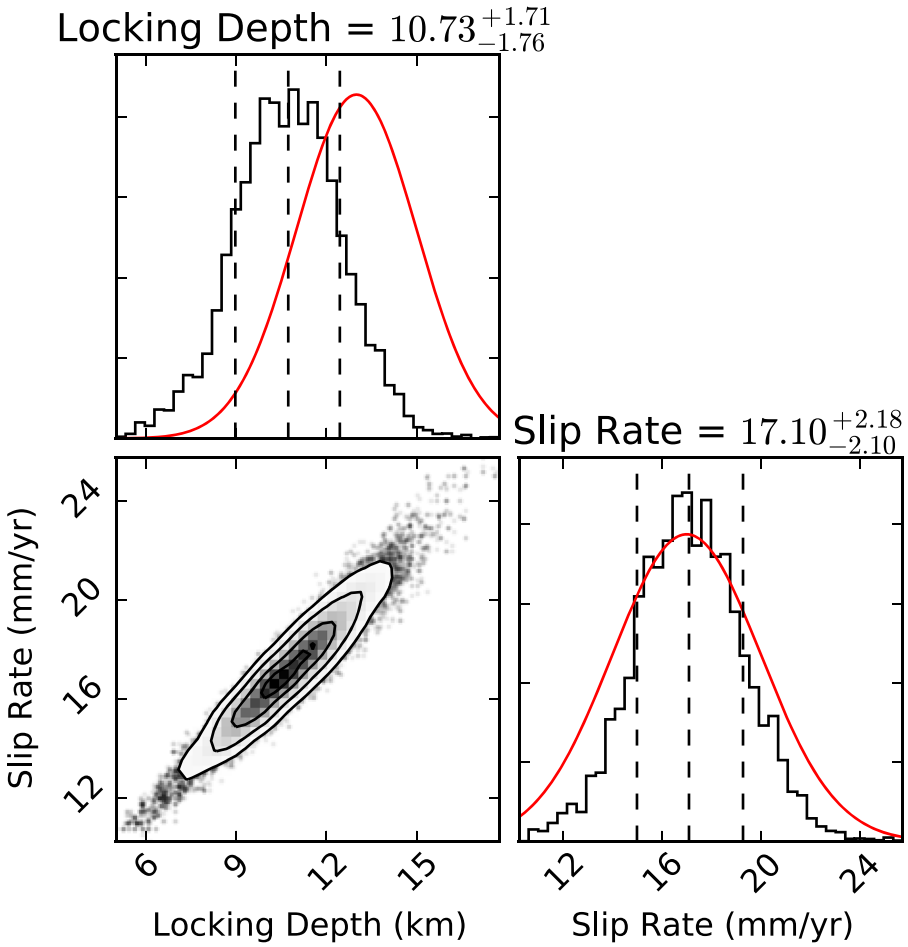

Figure 6. Results of arctangent modeling at Lake San Andreas. The black histograms show posterior probability distributions for the slip rate and locking depth. The red curves show the prior distributions derived from UCERF-3. The lower left plot shows the trade-off between slip rate and locking depth.

3. Results

3.1. Black Mountain Modeling Results

The fault-parallel GPS velocities for the Black Mountain data set are shown in Figure 3a, together with the modeling results for each candidate model of deformation. Across the 12 km of fault-perpendicular distance spanned in this data set, we see a fault-parallel velocity change of about 5 mm/yr. The fault-perpendicular velocities for these GPS data are all less than 1 mm/yr and show no systematic trend. The SAF is located at $x = 0$ in Figures 3a and 3b.

When we search for best fitting model parameters for this data set using the MCMC approach, we find preferred values for locking depth and slip rate at about 13 km and 17 mm/yr (Figure 4) under the homogeneous elastic half-space model. The posterior probability distributions for both parameters are in strong agreement with the prior distributions from UCERF-3. There is a trade-off between slip rate and locking depth (Figure 4, lower left), which is a common feature that *Lisowski et al.* [1991] and others have noted in the problem of slip rate and locking depth estimation from geodetic data, especially in the near field.

The results of the modeling using an asymmetric arctangent model were very similar to the results of the pure arctangent model (shown in detail in the supporting information Figure S2). In our modeling efforts, the preferred values for the asymmetry parameter were always very close to 0.5, indicating that this GPS data set does not support a contrast in shear modulus across the fault zone. Furthermore, the asymmetry coefficient

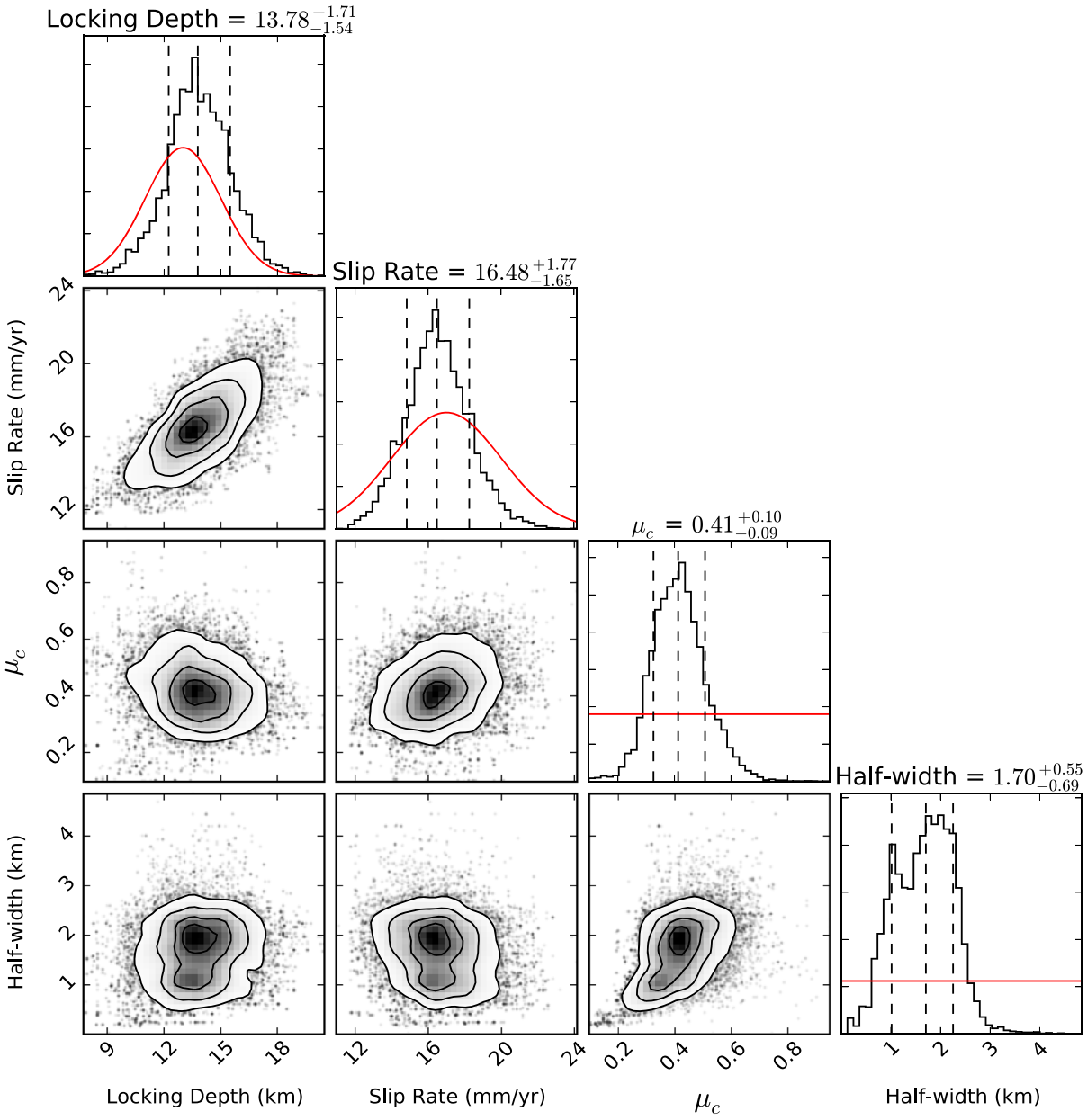

Figure 7. Results of CFZ modeling at Lake San Andreas. The graphs are similar to Figure 5 but for the Lake San Andreas data set. The prior distributions chosen for each parameter are shown in red.

does not have any strong trade-offs with the other parameters. This model does not provide substantially better fits to the data than the homogeneous elastic half-space model.

Finally, the results of the CFZ model are shown in the posterior distributions of Figure 5. This model produced best fitting slip rates of about 16 mm/yr and best fitting locking depths of about 14 km, as shown in the black histograms. The preferred values for compliance contrast μ_c of the fault zone are between 0.6 and 1, and the width of the CFZ is poorly constrained by the current data.

The poor constraints on the width of the CFZ (lower plots in Figure 5) are in part due to the fact that most of the preferred values for the normalized elastic modulus of the fault zone are close to 1. When the rigidity in the fault zone is relatively high, such as in these models, the fault zone deforms much like a homogeneous elastic half-space regardless of the width of the CFZ. In this case, the width of the fault zone has little effect on the resulting deformation.

Table 1. Summary of Bayes Factor Comparisons

Study Area	Model 1	Model 2	Bayes Factor	Interpretation
Black Mountain	Arctangent	Asymmetric	12.711	Strong preference for Arctangent
Black Mountain	Arctangent	CFZ	7.462	Strong preference for Arctangent
Lake San Andreas	Arctangent	Asymmetric	18.152	Very strong preference for Arctangent
Lake San Andreas	Arctangent	CFZ	0.002	Very strong preference for CFZ

3.2. Lake San Andreas Modeling Results

For Lake San Andreas, the fault-parallel GPS velocities and the three best fitting candidate models are shown in Figure 3b. This data set, which spans 18 km of fault-normal distance, shows a fault-parallel velocity change of about 8 mm/yr. All GPS measurements except one show fault-perpendicular velocities less than 1 mm/yr with no systematic patterns. Station SERR shows a fault-perpendicular velocity of 1.3 mm/yr (see section 4 for more on this measurement).

Figure 6 depicts the slip rate and locking depth results under the arctangent model. The preferred parameter values for this model were slip rates of about 17 mm/yr and locking depths of about 11 km, which is shallower than the UCERF-derived prior distribution centered at 13 km (shown by the red curve). This is also shallower than the depth extent of microseismicity in the area (about 14 km; see Figure 8).

Like the Black Mountain data set, the Lake San Andreas data set did not provide any convincing evidence for asymmetry in the elastic modulus across the fault. The results of this model produced asymmetry values near 0.5, resulting in nearly identical results to the homogeneous half-space model (see supporting information Figure S3).

The CFZ modeling at Lake San Andreas (Figure 7) indicates a best fit shear modulus that is reduced in the fault zone compared to the surrounding rock. The best fitting slip rates of about 16 mm/yr and locking depths of about 14 km are similar to the posterior distributions for slip rate and locking depth from the Black Mountain data set, but the CFZ parameters are quite different. The preferred values for the compliance ratio of the fault zone μ_c are about 0.4, and the half width of the CFZ is constrained between 1 and 2.25 km, with highest probability values around 1.7 km. The inferred total width of the CFZ is 3.4 +1.1/−1.4 km.

3.3. Model Comparisons

For each study area, we compared the arctangent model to the asymmetric and CFZ models using the Bayes factor (Table 1). For Black Mountain, we found that the two-parameter arctangent model was able to explain the data as well as the alternative three-parameter (asymmetric) or four-parameter (CFZ) models and that the Bayes factor was substantially greater than 1 in each comparison. We would expect such a result because the three models only produce slightly different fits (Figure 3a), and the Bayes factor, when given similar alternatives, tends to select the simplest model.

On the other hand, for Lake San Andreas, the CFZ model was strongly preferred over the arctangent model, as shown by the Bayes factor for this comparison being much less than 1. The asymmetric model was again not the preferred choice for explaining the data.

4. Discussion

The major result of our analysis is that geodetic measurements support the presence of a CFZ at Lake San Andreas but provide little support for a CFZ at Black Mountain. These results are somewhat different from the results of *Chen and Freymueller* [2002], who previously investigated the SAF and found geodetic evidence for CFZs at both of these locations. The values from *Chen and Freymueller* [2002] are presented in terms of a single shear strain rate measured by EDM and assumed to be representative of the entire fault zone. For straightforward comparison with their work, we converted our GPS velocity profiles into shear strain rates. We collected all fault-parallel velocities within 3 km of the fault, where the shear strain rate is 95–100% of the peak shear strain rate (utilizing nine GPS/EDM velocities in each region). We computed the shear strain rate from the slope of a linear trend fit to the GPS profile using weighted least squares.

At Black Mountain, we find shear strain rates that are near the low end of the 1 sigma confidence intervals presented in *Chen and Freymueller* [2002]. The previous study reports a shear strain rate of 0.316 ± 0.06 microstrain per year, while we find lower shear strain rates of 0.236 ± 0.05 microstrain per year.

As *Chen and Freymueller* [2002] noted, we would expect about 0.208 microstrain per year from a homogeneous half-space (assuming reasonable values of 17 mm/yr slip rate and 13 km locking depth). Our measurements are much closer to this value than the previous study's. It seems that GPS measurements collected over the last 20 years refine our picture of SAF deformation at Black Mountain to one with lower strain rates. This shift is likely due to an improvement in data quality and coverage rather than a temporal change in slip rate or locking depth.

At Lake San Andreas, the EDM measurements from *Chen and Freymueller* [2002] showed high shear strain rates of 0.366 ± 0.095 microstrain per year, and our measurements are in very close agreement (0.340 ± 0.09 microstrain per year). The Bayes factor analysis shows that a CFZ model is strongly preferred over a homogeneous half-space model in order to explain the geodetic data.

The physical parameters we infer for the CFZ at Lake San Andreas, including a CFZ width of about 3.4 +1.1/−1.4 km and a 60% reduced elastic modulus, are similar to other geodetically inferred CFZs in the literature. For example, *Hamiel and Fialko* [2007] find CFZs of approximately 2–3 km in width and 60–70% reductions in elastic modulus for faults in the North Anatolian Fault system. *Fialko* [2004] finds compliant zones around the Calico and Pinto Mountain Faults in the Mojave Desert characterized by widths of 2 km and 50% reductions of elastic modulus. Such CFZs may be common for crustal faults with extensive damage sustained over many earthquake cycles, but more research is required to characterize these zones around other major faults.

The introduction of a CFZ into the deformation modeling at Lake San Andreas places the geodetically inferred locking depth at about 14 km depth, whereas modeling with an elastic half-space model results in a shallower locking depth of about 11 km (Figures 6 and 7). The 14 km locking depth at Lake San Andreas is more closely aligned with the depth extent of local microseismicity, shown in Figure 8 from the double-differenced catalog of *Waldhauser and Schaff* [2008]. At Black Mountain on the other hand, small earthquakes are observed to about 12 km, which is already close to the inferred geodetic locking depth under the homogeneous half-space model (13 km in Figure 4). The addition of a CFZ into the model is not necessary to match the depth of microseismicity. We note that the depth of microseismicity at our study areas is likely a useful but not definitive indication of the true locking depth. The geodetic locking depth of a fault need not always agree with the seismogenic depth, which may undergo variations throughout the earthquake cycle [*Jiang and Lapusta*, 2016]. However, *Smith-Konter et al.* [2011] found that on the southern SAF, the geodetic and seismogenic locking depths most often agree to within 2 km. With a CFZ model at the Lake San Andreas, we find agreement at or below this level.

At both Lake San Andreas and Black Mountain, we find that the asymmetric half-space model does not provide a better fit to the data than the simple arctangent model. This finding is not surprising given that we consider mostly near-field rather than far-field geodetic data, making our analysis less sensitive to asymmetry parameters simply due to the geometry of our networks [*Le Pichon et al.*, 2005]. In order to more thoroughly characterize the possible asymmetries in elastic parameters on the San Francisco Peninsula, we would need to obtain more geodetic data far to the east and west of the San Andreas Fault and construct a larger-scale model that includes nearby faults and trade-offs with slip rates on those faults. In one larger-scale model [*d'Alessio et al.*, 2005], the residuals show no obvious asymmetry, suggesting that the effects of asymmetric elastic heterogeneity in this region may be small.

Even with our relatively dense data set of near-field measurements, the specific placement of GPS benchmarks still somewhat limits our ability to infer fault zone properties and kilometer-scale features. With only 10–15 GPS benchmarks at each field site, we are subject to effects from potential outliers and small sample sizes. For example, the Lake San Andreas data set has a station (SERR, located about 2.2 km west of the SAF in Figure 6) that appears to have an unusually high fault-parallel velocity. This campaign measurement is based on one observation in 1997 and one observation in 2015, so it is possible that measurement errors at either epoch could have affected the velocity. However, earlier EDM measurements also show this benchmark moving unusually fast in the fault-parallel direction, with the GPS velocity 0.8 mm/yr faster than the EDM measurement. Nontectonic explanations for the velocity could include site disturbances or landsliding beneath the benchmark, but we did not see evidence for that in the field (the benchmark was in good condition at the top of a hill). Therefore, because we lacked field evidence to correct the motion of the benchmark, we chose to include this data point in our modeling efforts rather than exclude it outright. Removing this data point from our parameter estimation resulted in approximately the same estimates for CFZ width, rigidity,

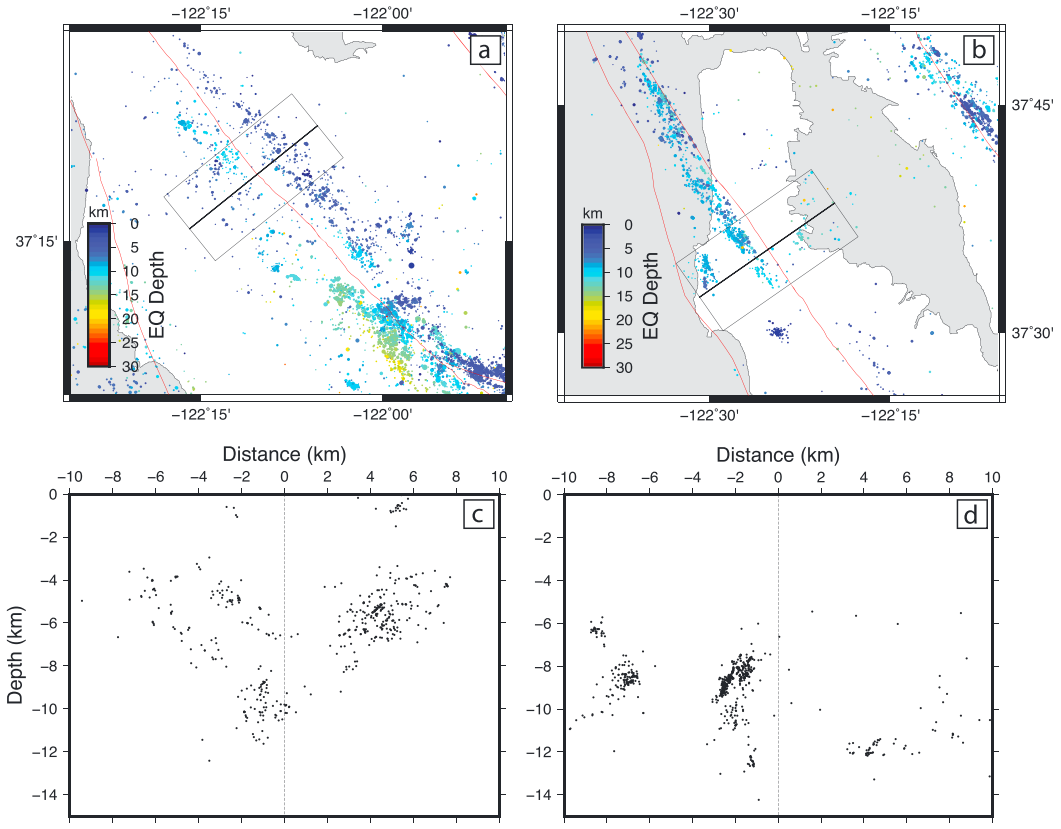

Figure 8. Microseismicity at (a) Black Mountain and (b) Lake San Andreas. (c and d) The profiles of microseismicity with depth drawn across each field site. The seismicity data are from the double-differenced catalog (1984–2015) accessed through the Northern California Earthquake Data Center. Mean 95% relative location errors in the double-differenced catalog are 0.06 km in the vertical and 0.04 km in the horizontal.

locking depth, and slip rate but with lower significance (see Table S3 in the supporting information for analysis). With a denser spacing of geodetic measurements in the future, we could avoid potential biases from such data points, which might include nontectonic signals we are otherwise unable to separate from the fault-related deformation.

InSAR data may be able to generate the desired dense profiles of deformation in the future. To gain higher spatial resolution, we analyzed the available InSAR data from *Chaussard et al.* [2015] for evidence of CFZ-related localization of deformation. This estimate of fault-parallel velocities is derived from InSAR alone with scenes selected to maximize coherence over the Santa Clara Valley, so it is not adjusted to optimize for the specific velocity fields of our study regions. Nonetheless, the InSAR data generally show very good agreement with the GPS data in both regions (Figure 9). The data are limited to the west of the SAF due to decorrelation from vegetation but are more coherent in the populated areas east of the fault. We were unable to directly resolve features as subtle as CFZs in the InSAR data for either field area. The deformation signals that indicate the presence of a CFZ around the SAF are about 1 mm/yr in magnitude, which is the same order as the scatter in the InSAR data. Further work, including with future InSAR missions that have L band measurements with shorter repeat times, may be able to help resolve CFZs with InSAR in this and other regions in the future.

We note that the MCMC analysis and the Bayes factor comparison between the candidate models provide a useful framework for distinguishing between models but do not address the assumptions in those models that may be fundamentally wrong. For example, we do not model off-fault inelastic deformation, which may play a role in this region given the presence of off-fault microseismicity at both study areas (Figures 8c and 8d). *Lindsey et al.* [2014] suggest that a fault's tectonic setting within a restraining or releasing bend can influence the fault's style of off-fault deformation and localized surface creep. In their work, releasing bends are observed to have more off-fault deformation than restraining bends. At Lake San Andreas, located along a releasing bend of the SAF, the degree of off-fault deformation from either folding or distributed brittle

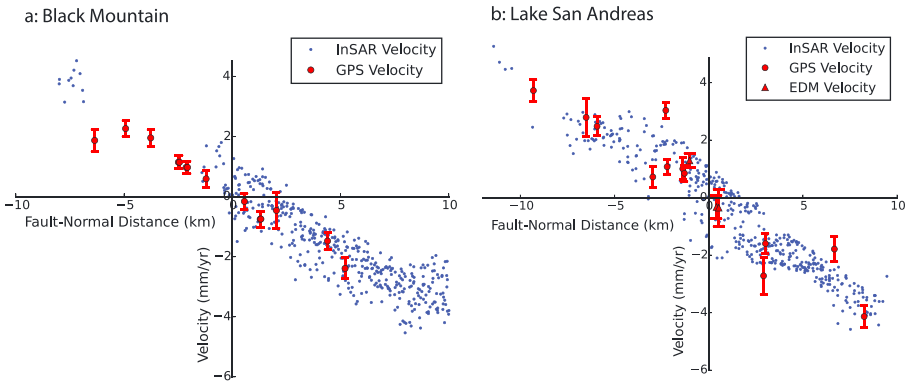

Figure 9. GPS/EDM and InSAR velocities at (a) Black Mountain and (b) Lake San Andreas. InSAR data are from *Chaussard et al.* [2015], where velocities are obtained from ascending and descending satellite viewing geometries. The line-of-site velocities are projected into the horizontal assuming that the horizontal component is only due to fault-parallel movement.

faulting is an important question to address in future models. However, it is difficult to address with the currently available GPS and InSAR data. With ever increasing quality and spatial density of InSAR data, especially west of the SAF in highly vegetated areas, we hope to address these important questions in future work.

A related factor that we do not model in this work is a dipping SAF. Studies such as *Lindsey and Fialko* [2013] show that the dip of a fault in an elastic half-space can affect the geodetically inferred slip rate and locking depth, and *Fialko* [2006] shows that the elastic asymmetry parameter inferred across a fault and the dip of the fault trade off with one another. The location of the CFZ relative to the surface trace and the deep dislocation may also have effects on modeled deformation. While fault dip is an important factor in modeling geodetic data, we suggest that the effects of fault dip in these two study areas are probably small. There is seismicity away from the surface trace of the SAF in both study areas, but *Zoback et al.* [1999] find that these events have dip-slip mechanisms and are likely related to off-fault seismicity rather than the main SAF. A number of tomographic studies also find that the SAF is a steeply dipping to vertical feature in both study regions [*Parsons and Zoback*, 1997; *Thurber et al.*, 2007].

We also do not model shallow creep on the SAF, but we consider this unlikely to be a major factor on the SAF due to the lack of creep detected on creepmeters just north of Lake San Andreas [*Lienkaemper et al.*, 2014], the high interseismic coupling estimated in UCERF-3 [*Field et al.*, 2014], and the lack of localized microseismicity on the fault.

The results of our study have implications for how CFZs form over the lifetimes of crustal faults. In the context of earlier studies on CFZs along the northern SAF [e.g., *Chen and Freymueller*, 2002; *Jolivet et al.*, 2009], our results suggest that there is strong variability in fault zone structure within the San Francisco Bay Area. From south to north, there is little to no evidence for a CFZ at Black Mountain, strong evidence at Lake San Andreas, little evidence at Point Reyes, and strong evidence at Bodega Bay, just 30 km north of Point Reyes. Our data at the two southern field sites allow us to speculate on what factors might control the development of these features in some places and not others.

Based on the data at Black Mountain and Lake San Andreas, we suggest that fault lithology is an important factor in CFZ formation, perhaps even more important in this case than fault age or cumulative displacement. At Lake San Andreas, although there is only 23 km of cumulative fault displacement on a relatively young branch of the SAF, there is evidence for a well-developed CFZ. A CFZ is made of extensively damaged rocks; thus, the lithology of the fault zone, and specifically how the rocks sustain damage, should play a major role in CFZ formation. The lithology of the Lake San Andreas region (Franciscan rocks adjacent to other Franciscan rocks) may play a large role in determining the type of CFZs we infer from geodetic data. In contrast, Black Mountain is a more mature fault zone bounded on the west by rigid Salinian rocks, but it does not display evidence for a CFZ. A recent study on postseismic deformation and afterslip in northern California [*Floyd et al.*, 2016] has also found evidence that changes in fault behavior can be correlated with first-order changes in fault lithology. More research is needed to understand the effects of lithologic contrasts on fault zone development and behavior.

The tectonic setting may also play a role in the type of damage sustained by the fault zone. In our study areas, the transpressional region at Black Mountain shows less evidence for a CFZ than the transtensional section near Lake San Andreas. The morphology of the SAF at the transtensional region, where we infer the presence of a CFZ, includes a low-lying 1–2 km wide "rift valley" with two lakes, which could reflect an easily eroded damage zone surrounding the fault. The reduction in normal stress associated with the transtensional regime at Lake San Andreas could also play a role in the extent of damage structures and the resulting topographic expression of the fault.

Our study of fault zone properties has potential implications for the coseismic behavior of faults. For example, *Dolan and Haravitch* [2014] show that the degree of localized surface slip during strike-slip earthquakes is correlated with the structural maturity of faults. They find a relationship between the cumulative displacement on a fault and the amount of distributed slip or "shallow slip deficit" during earthquakes. Our results imply that cumulative displacement may be only one of several factors that define fault maturity, with fault lithology and tectonic setting also playing a significant role.

Recently, *Huang et al.* [2016] reported a possible connection between faults with CFZs and faults that can sustain supershear ruptures. In light of this, our results are particularly interesting given geodetic and seismic evidence that the 1906 earthquake, which ruptured at both of our study areas, may have been a supershear rupture along at least some of its length [*Song et al.*, 2008]. Further observational and theoretical studies are required in order to better understand the connection between the fault zone damage structures in the San Francisco Bay Area and the types of ruptures they can sustain.

Acknowledgments
The authors thank the Associate Editor, two anonymous reviewers, and Romain Jolivet for their helpful comments that greatly improved the manuscript. We also thank I. Johanson for early field work and insightful discussions on this project. The authors are grateful to Chelsea Willett, Robert Martin-Short, Mong-Han Huang, Brent Delbridge, Alizee Dubois, Leighton Watson, and Joseph Schiavone for their help in the field, as well as to the Mid-Peninsula Open Space District, the Santa Clara County Parks and Recreation Department, and the San Francisco Public Utilities Commission for making the field work possible. During this project, K.M. was supported through the Berkeley Fellowship for Graduate Study. The GPS velocities used in this project can be found in the supporting information. The raw campaign data collected as part of this project are archived at the UNAVCO Data Center through doi 10.7283/T5BV7DZQ and doi 10.7283/T5736P7Q. We thank the Plate Boundary Observatory and the United States Geological Survey for providing continuous and campaign geodetic data for this project. Some GPS data for this study come from the Bay Area Regional Deformation Network (BARD), doi:10.7932/BARD, operated by the UC Berkeley Seismological Laboratory, which is archived at the Northern California Earthquake Data Center (NCEDC), doi: 10.7932/NCEDC. Earthquake catalog data products for this study were accessed through the Northern California Earthquake Data Center (NCEDC), doi:10.7932/NCEDC. We thank the NASA for support through grant NNX12AQ32G.

5. Conclusion

Using new geodetic measurements, we infer the presence of a compliant fault zone around the northern SAF at Lake San Andreas, characterized by a width of about 3.4 +1.1/−1.4 km and a 60% reduction in shear modulus; we also infer a slip rate of about 16 mm/yr and locking depth of 14 km. However, we do not find evidence for a similar CFZ feature at Black Mountain. We find that the best fitting model for the Black Mountain GPS data contains a homogeneous elastic half-space with the SAF slipping at about 17 mm/yr and locked to 13 km depth.

This result, highlighting two nearby but lithologically different segments of the SAF, suggests that fault lithology may influence the formation of CFZs in this region. However, questions remain about the distribution and characteristics of fault zones in the larger SAF system and on other faults. In order to more fully understand CFZs in northern California and variations in CFZ properties along faults, further geodetic measurements are necessary. We also suggest that other geophysical methods, including seismic studies of fault zone guided waves [e.g., *Cochran et al.*, 2009], are needed to characterize the fault zones of the northern SAF. Given that geodetic data suggest the presence of a CFZ at Lake San Andreas, a study of this kind at Lake San Andreas may be a promising avenue for future work on CFZs.

References

Anderson, R. S. (1990), Evolution of the northern Santa Cruz Mountains by advection of crust past a San Andreas fault bend, *Science*, *249*(4967), 397–401, doi:10.1126/science.249.4967.397.

Barbot, S., Y. Fialko, and D. Sandwell (2008), Effect of a compliant fault zone on the inferred earthquake slip distribution, *J. Geophys. Res.*, *113*, B06404, doi:10.1029/2007JB005256.

Bayes, T. (1763), An essay towards solving a problem in the doctrine of chances, *Philos. Trans.*, *53*, 370–418.

Ben-Zion, Y., F. L. Vernon, Y. Ozakin, D. Zigone, Z. E. Ross, H. Meng, M. White, J. Reyes, D. Hollis, and M. Barklage (2015), Basic data features and results from a spatially dense seismic array on the San Jacinto fault zone, *Geophys. J. Int.*, *202*(1), 370–380, doi:10.1093/gji/ggv142.

Blake, M. C., and D. L. Jones (1974), Origin of Franciscan Melanges in Northern California, in *Modern And Ancient Geosynclinal Sedimentation*, edited by R. H. Dott and R. H. Shaver, Soc. Econ. Paleont. Mineral. Spec. Publ., 19, pp. 11–48, Tulsa, Okla.

Brocher, T. M. (2005), Compressional and shear wave velocity versus depth in the San Francisco bay area, California: Rules for USGS bay area velocity model 05.0.0, *U.S. Geol. Surv. Open File Rep., 2005-1317*.

Bürgmann, R., R. Arrowsmith, T. Dumitru, and R. McLaughlin (1994), Rise and fall of the southern Santa Cruz Mountains, California, from fission tracks, geomorphology, and geodesy, *J. Geophys. Res.*, *99*(B10), 20,181–20,202, doi:10.1029/94JB00131.

Chaussard, E., R. Bürgmann, H. Fattahi, C. W. Johnson, R. Nadeau, T. Taira, and I. Johanson (2015), Interseismic coupling and refined earthquake potential on the Hayward-Calaveras fault zone, *J. Geophys. Res. Solid Earth*, *120*, 8570–8590, doi:10.1002/2015JB012230.

Chen, Q., and J. T. Freymueller (2002), Geodetic evidence for a near-fault compliant zone along the San Andreas Fault in the San Francisco Bay Area, *Bull. Seismol. Soc. Am.*, *92*(2), 656–671, doi:10.1785/0120010110.

Cochran, E. S., Y.-G. Li, P. M. Shearer, S. Barbot, Y. Fialko, and J. E. Vidale (2009), Seismic and geodetic evidence for extensive, long-lived fault damage zones, *Geology*, *37*(4), 315–318, doi:10.1130/G25306A.1.

d'Alessio, M. A., I. A. Johanson, R. Bürgmann, D. A. Schmidt, and M. H. Murray (2005), Slicing up the San Francisco Bay Area: Block kinematics and fault slip rates from GPS-derived surface velocities, *J. Geophys. Res.*, *110*, B06403, doi:10.1029/2004JB003496.

Dolan, J. F., and B. D. Haravitch (2014), How well do surface slip measurements track slip at depth in large strike-slip earthquakes? The importance of fault structural maturity in controlling on-fault slip versus off-fault surface deformation, *Earth Planet. Sci. Lett.*, *388*, 38–47.

Fialko, Y. (2004), Probing the mechanical properties of seismically active crust with space geodesy: Study of the coseismic deformation due to the 1992 M_w7.3 Landers (southern California) earthquake, *J. Geophys. Res.*, *109*, B03307, doi:10.1029/2003JB002756.

Fialko, Y. (2006), Interseismic strain accumulation and the earthquake potential on the southern San Andreas fault system, *Nature*, *441*(7096), 968–971, doi:10.1038/nature04797.

Field, E. H., et al. (2014), Uniform California earthquake rupture forecast, version 3 (UCERF3)—The time-independent model, *Bull. Seismol. Soc. Am.*, *104*(3), 1122–1180, doi:10.1785/0120130164.

Floyd, M. A., et al. (2016), Spatial variations in fault friction related to lithology from rupture and afterslip of the 2014 South Napa, California, earthquake, *Geophys. Res. Lett.*, *43*, 6808–6816, doi:10.1002/2016GL069428.

Hamiel, Y., and Y. Fialko (2007), Structure and mechanical properties of faults in the North Anatolian Fault system from InSAR observations of coseismic deformation due to the 1999 Izmit (Turkey) earthquake, *J. Geophys. Res.*, *112*, B07412, doi:10.1029/2006JB004777.

Hengesh, J. V., and J. Wakabayashi (1995), Dextral translation and progressive emergence of the Pleistocene Merced basin and implications for timing of initiation of the San Francisco Peninsula segment of the San Andreas fault, in *Recent Geologic Studies in the San Francisco Bay Area*, vol. 76, edited by E. M. Sangines, D. W. Anderson, and A. B. Buising, Pac. Sect. Soc. of Econ. Paleontol. and Mineral. Publ., 76, pp. 47–53, Los Angeles, Calif.

Herring, T. A., R. W. King, M. A. Floyd, and S. C. McClusky (2015), *Introduction to GAMIT/GLOBK, Release 10.6*. [Available at http://www-gpsg.mit.edu/~simon/gtgk/Intro_GG.pdf.]

Huang, Y., J.-P. Ampuero, and D. V. Helmberger (2016), The potential for supershear earthquakes in damaged fault zones—Theory and observations, *Earth Planet. Sci. Lett.*, *433*, 109–115, doi:10.1016/j.epsl.2015.10.046.

Jachens, R. C., and M. L. Zoback (1999), The San Andreas Fault in the San Francisco Bay region, California: Structure and kinematics of a young plate boundary, *Int. Geol. Rev.*, *41*(3), 191–205, doi:10.1080/00206819909465139.

James, E. W. (1992), Cretaceous metamorphism and plutonism in the Santa Cruz Mountains, Salinian block, California, and correlation with the southernmost Sierra Nevada, *Geol. Soc. Am. Bull.*, *104*(10), 1326–1339, doi:10.1130/0016-7606(1992)104.

Jeffreys, H. (1961), *The Theory of Probability*, 3rd ed., Oxford Univ. Press.

Jiang, J., and N. Lapusta (2016), Deeper penetration of large earthquakes on seismically quiescent faults, *Science*, *352*(6291), 1293–1297, doi:10.1126/science.aaf1496.

Jolivet, R., R. Bürgmann, and N. Houlié (2009), Geodetic exploration of the elastic properties across and within the northern San Andreas Fault zone, *Earth Planet. Sci. Lett.*, *288*(1–2), 126–131, doi:10.1016/j.epsl.2009.09.014.

Kruschke, J. (2015), *Doing Bayesian Data Analysis: A Tutorial With R, JAGS, and Stan*, 2nd ed., Academic Press, London.

Le Pichon, X., C. Kreemer, and N. Chamot-Rooke (2005), Asymmetry in elastic properties and the evolution of large continental strike-slip faults, *J. Geophys. Res.*, *110*, B03405, doi:10.1029/2004JB003343.

Li, Y.-G., J. E. Vidale, and E. S. Cochran (2004), Low-velocity damaged structure of the San Andreas Fault at Parkfield from fault zone trapped waves, *Geophys. Res. Lett.*, *31*, L12S06, doi:10.1029/2003GL019044.

Lienkaemper, J. J., F. S. McFarland, R. W. Simpson, and S. J. Caskey (2014), Using surface creep rate to infer fraction locked for sections of the San Andreas Fault system in northern California from alignment array and GPS data, *Bull. Seismol. Soc. Am.*, *104*(6), 3094–3114, doi:10.1785/0120140117.

Lindsey, E. O., and Y. Fialko (2013), Geodetic slip rates in the southern San Andreas Fault system: Effects of elastic heterogeneity and fault geometry, *J. Geophys. Res. Solid Earth*, *118*, 689–697, doi:10.1029/2012JB009358.

Lindsey, E. O., V. J. Sahakian, Y. Fialko, Y. Bock, S. Barbot, and T. K. Rockwell (2013), Interseismic strain localization in the San Jacinto Fault zone, *Pure Appl. Geophys.*, *171*(11), 2937–2954, doi:10.1007/s00024-013-0753-z.

Lindsey, E. O., Y. Fialko, Y. Bock, D. T. Sandwell, and R. Bilham (2014), Localized and distributed creep along the southern San Andreas Fault, *J. Geophys. Res. Solid Earth*, *119*, 7909–7922, doi:10.1002/2014JB011275.

Lisowski, M., J. C. Savage, and W. H. Prescott (1991), The velocity field along the San Andreas Fault in central and southern California, *J. Geophys. Res.*, *96*(B5), 8369–8389, doi:10.1029/91JB00199.

Mattinson, J. M. (1978), Age, origin, and thermal histories of some plutonic rocks from the Salinian block of California, *Contrib. Mineral. Petrol.*, *67*(3), 233–245, doi:10.1007/BF00381451.

Metropolis, N., A. W. Rosenbluth, M. N. Rosenbluth, A. H. Teller, and E. Teller (1953), Equation of state calculations by fast computing machines, *J. Chem. Phys.*, *21*(6), 1087–1092, doi:10.1063/1.1699114.

Parsons, T., and M. L. Zoback (1997), Three-dimensional upper crustal velocity structure beneath San Francisco Peninsula, California, *J. Geophys. Res.*, *102*(B3), 5473–5490, doi:10.1029/96JB03222.

Patil, A., D. Huard, and C. J. Fonnesbeck (2010), PyMC: Bayesian stochastic modelling in Python, *J. Stat. Software*, *35*(4), 1–81.

Powell, R. E. (1993), Balanced palinspastic reconstruction of pre-late Cenozoic paleogeology, southern California: Geologic and kinematic constraints on evolution of the San Andreas fault system, in *The San Andreas Fault System: Displacement, Palinspastic Reconstruction, and Geologic Evolution*, pp. 1–106, Boulder, Colo.

Prescott, W. H. (1981), The determination of displacement fields from geodetic data along a strike slip fault, *J. Geophys. Res.*, *86*(B7), 6067–6072, doi:10.1029/JB086iB07p06067.

Reinoza, C., F. Jouanne, F. A. Audemard, M. Schmitz, and C. Beck (2015), Geodetic exploration of strain along the El Pilar Fault in northeastern Venezuela, *J. Geophys. Res. Solid Earth*, *120*, 1993–2013, doi:10.1002/2014JB011483.

Rybicki, K., and K. Kasahara (1977), A strike-slip fault in a laterally inhomogeneous medium, *Tectonophysics*, *42*(2), 127–138, doi:10.1016/0040-1951(77)90164-0.

Savage, J. C., and R. O. Burford (1973), Geodetic determination of relative plate motion in central California, *J. Geophys. Res.*, *78*(5), 832–845, doi:10.1029/JB078i005p00832.

Scholz, C. H. (1985), The Black Mountain asperity: Seismic hazard of the southern San Francisco Peninsula, California, *Geophys. Res. Lett.*, *12*(10), 717–719, doi:10.1029/GL012i010p00717.

Segall, P. (2010), *Earthquake and Volcano Deformation*, student ed., Princeton Univ. Press.

Smith-Konter, B. R., D. T. Sandwell, and P. Shearer (2011), Locking depths estimated from geodesy and seismology along the San Andreas Fault System: Implications for seismic moment release, *J. Geophys. Res.*, *116*, B06401, doi:10.1029/2010JB008117.

Song, S. G., G. C. Beroza, and P. Segall (2008), A unified source model for the 1906 San Francisco earthquake, *Bull. Seismol. Soc. Am.*, *98*(2), 823–831, doi:10.1785/0120060402.

Thurber, C. H., T. M. Brocher, H. Zhang, and V. E. Langenheim (2007), Three-dimensional P wave velocity model for the San Francisco Bay region, California, *J. Geophys. Res.*, *112*, B07313, doi:10.1029/2006JB004682.

Waldhauser, F., and D. P. Schaff (2008), Large-scale relocation of two decades of northern California seismicity using cross-correlation and double-difference methods, *J. Geophys. Res.*, *113*, B08311, doi:10.1029/2007JB005479.

Xue, L., E. E. Brodsky, J. Erskine, P. M. Fulton, and R. Carter (2016), A permeability and compliance contrast measured hydrogeologically on the San Andreas Fault, *Geochem. Geophys. Geosyst.*, *17*(3), 858–871, doi:10.1002/2015GC006167.

Zoback, M. L., R. C. Jachens, and J. A. Olson (1999), Abrupt along-strike change in tectonic style: San Andreas Fault zone, San Francisco Peninsula, *J. Geophys. Res.*, *104*(B5), 10,719–10,742, doi:10.1029/1998JB900059.